

# The Scale-Dependence of Halo Assembly Bias

Tomomi Sunayama<sup>1,2</sup>, Andrew P. Hearin<sup>2</sup>, Nikhil Padmanabhan<sup>1,2</sup>, Alexie Leauthaud<sup>3</sup>

<sup>1</sup>*Department of Physics, Yale University, P.O. Box 208120, New Haven, CT*

<sup>2</sup>*Yale Center for Astronomy & Astrophysics, Yale University, New Haven, CT*

<sup>3</sup>*Kavli IPMU (WPI), UTIAS, The University of Tokyo, Kashiwa, Chiba 277-8583, Japan*

23 September 2015

## ABSTRACT

The two-point clustering of dark matter halos is influenced by halo properties besides mass, a phenomenon referred to as *halo assembly bias*. Using the depth of the gravitational potential well,  $V_{\max}$ , as our secondary halo property, in this paper we present the first study of the scale-dependence assembly bias. In the large-scale linear regime,  $r \gtrsim 10\text{Mpc}/h$ , our findings are in keeping with previous results. In particular, at the low-mass end ( $M_{\text{vir}} < M_{\text{coll}} \approx 10^{12.5} M_{\odot}/h$ ), halos with high- $V_{\max}$  show stronger large-scale clustering relative to halos with low- $V_{\max}$  of the same mass; this trend weakens and reverses for  $M_{\text{vir}} \gtrsim M_{\text{coll}}$ . In the nonlinear regime, assembly bias in low-mass halos exhibits a pronounced scale-dependent “bump” at  $500\text{kpc}/h - 5\text{Mpc}/h$ , a new result. This feature weakens and eventually vanishes for halos of higher mass. We show that this scale-dependent signature can primarily be attributed to a special subpopulation of *ejected halos*, defined as present-day host halos that were previously members of a higher-mass halo at some point in their past history. A corollary of our results is that galaxy clustering on scales of  $r \sim 1 - 2\text{Mpc}/h$  can be impacted by up to  $\sim 15\%$  by the choice of the halo property used in the halo model, even for stellar mass-limited samples.

## 1 INTRODUCTION

The halo model provides a connection between dark matter halos and galaxies, and it has been remarkably successful in describing observations of galaxy clustering (Seljak 2000; Mo et al. 2010, for a recent review). In particular, the Halo Occupation Distribution (HOD) (Berlind & Weinberg 2002; Berlind et al. 2003) and the Conditional Luminosity Function (CLF) (Yang et al. 2003) are the two most widely used models of the galaxy-halo connection. These models start from the assumption that halo mass completely determines the galaxy occupation statistics. In order to populate halos with galaxies, the HOD specifies the probability  $P(N|M)$  that a halo with mass  $M$  hosts  $N$  galaxies, while the CLF models the mean abundance  $\Phi(L|M)$  of galaxies with luminosity  $L$  in halos of mass  $M$ . These two models are interchangeable; integrating the CLF over luminosity yields an HOD. Both models have been applied extensively to observations in order to study the galaxy-halo connection (Magliocchetti & Porciani 2003; Zehavi et al. 2005; Yang et al. 2005; Zheng et al. 2007; van den Bosch et al. 2007; Zheng et al. 2009; Skibba 2009; Simon et al. 2009; Ross et al. 2010; Zehavi et al. 2011; Leauthaud et al. 2011, 2012; Geach et al. 2012; Parejko et al. 2013) as well as cosmology (Tinker et al. 2005; More et al. 2013; Cacciato et al. 2013; Mandelbaum et al. 2013).

However, the clustering of halos also exhibits a dependence on additional properties beyond their mass (Gao et al. 2005; Wechsler et al. 2006; Gao & White 2007; Li et al. 2008; Hahn et al. 2009), a phenomenon generically referred to as *halo assembly bias*. This can be traced back to the fact that halos of

the same mass in different environments have different assembly histories and cluster differently. Having different assembly histories also affects the internal structure of halos (Bullock et al. 2001; Wechsler et al. 2002; Hahn et al. 2007; Faltenbacher & White 2010). This, in turn, results in a clustering dependence on the structural properties of a halo, including the depth of its gravitational potential well, characterized by its maximum circular velocity  $V_{\max}$ . The present work revisits this manifestation of halo assembly bias, and extends it down to smaller scales ( $< 10h^{-1}\text{Mpc}$ ) than has been previously explored.

An alternative approach to connecting halos and galaxies is abundance matching (Kravtsov et al. 2004; Vale & Ostriker 2004; Tasitsiomi et al. 2004; Vale & Ostriker 2006; Conroy & Wechsler 2009; Guo et al. 2010; Simha et al. 2010; Neistein et al. 2010; Watson et al. 2012; Rodríguez-Puebla et al. 2012; Hearin et al. 2012; Kravtsov 2013; Saito et al. 2015). In its simplest form, abundance matching posits a monotonic relationship between a property of a galaxy (luminosity, stellar mass) and that of a halo (mass, potential well depth). By construction, such a relationship preserves the rank ordering of the galaxies and halos. The choice of the observationally-relevant halo property is a priori unknown; this uncertainty that can lead to significant systematic errors when using halo models to interpret galaxy clustering measurements (Zentner et al. 2013).

A recent parallel research effort has been revisiting the standard subdivision of dark matter halos into host/sub-halos, a classification that naturally depends on how the halo boundary is chosen. While the virial radius is the most commonly chosen definition, recent work has demonstrated that the environmen-

tal effects of halos extends well beyond the virial radius (Wetzel et al. 2014; Diemer & Kravtsov 2014; Adhikari et al. 2014; Wetzel & Nagai 2014; More et al. 2015). In particular, Wetzel et al. (2014) argue that these environmental effects are due to ejected subhalos which orbit beyond the virial radius of their hosts, and therefore get temporarily reclassified as host halos. These studies argue that a more physically motivated boundary is the “splashback radius” corresponding to the caustic from material just reaching its first apocentric passage. One of the chief results of the present work is that the halo assembly bias on small scales predominantly arises from this mis-classification.

The outline of this paper is as follows. Sec. 2 summarizes the simulations we use in this work. Sec. 3 presents our primary results - characterizing the dependence of the clustering of halos on  $V_{\max}$ ; Sec. 4 explores some of the implications of these results. We conclude in Sec. 5.

## 2 SIMULATIONS

We use the Bolshoi (Klypin et al. 2011a) and MultiDark simulations (Riebe et al. 2011; Prada et al. 2011)<sup>1</sup> in this work; the combination of these simulations allows us to span a large range in halo mass. We summarize key properties of these simulations here. Both simulations were run with the Adaptive Refinement Tree Code (Kravtsov et al. 1997; Gottloeber & Klypin 2008) assuming a flat  $\Lambda$ CDM model with density parameters  $\Omega_m = 0.27$ ,  $\Omega_\Lambda = 0.73$ ,  $\Omega_b = 0.0469$ , and  $\sigma_8 = 0.82$ ,  $n = 0.95$ ,  $h = 0.70$ . The Bolshoi simulation used  $2048^3$  particles in a  $250h^{-1}$ Mpc box with a force resolution of  $1h^{-1}$ kpc, giving a particle mass of  $1.35 \times 10^8 h^{-1} M_\odot$ , while the MultiDark simulation used  $2048^3$  particles in a  $1h^{-1}$ Gpc box with a force resolution of  $7h^{-1}$ kpc giving a particle mass of  $8.721 \times 10^9 h^{-1} M_\odot$ . Dark matter halos and subhalos are identified using the ROCKSTAR phase-space, temporal halo finder (Behroozi et al. 2013d) and merger trees are constructed using the CONSISTENT TREES (Behroozi et al. 2013c) procedures<sup>2</sup>. All of the results we consider here are at  $z = 0$ .

In what follows, we use the virial masses and maximum circular velocities (tagged “`mvir`” and “`vmax`”) directly from the halo catalogues. The halo mass and velocity functions start to show incompleteness at  $10^{10.4} h^{-1} M_\odot$  ( $\sim 200$  particles) for the Bolshoi simulation, and  $10^{12} h^{-1} M_\odot$  ( $\sim 100$  particles) for the MultiDark simulation. Below those masses, the halo mass distributions show unphysical drop-offs indicating incomplete mass resolution.

In addition to the standard classification of halos into host halos (not within the virial radius of a more massive halo) and subhalos (within the virial radius of a more massive halo), we further classify host halos into ejected and non-ejected halos. Ejected halos, also referred to as “backsplash” halos, are host halos whose main progenitor was classified, at some point in its merger tree history, as a subhalo. As we discuss below, these ejected halos have very different clustering properties compared to their non-ejected counterparts. The ejected fraction for the Bolshoi simulation is  $\sim 15.8\%$  at  $10^{11} h^{-1} M_\odot$ , and drops to

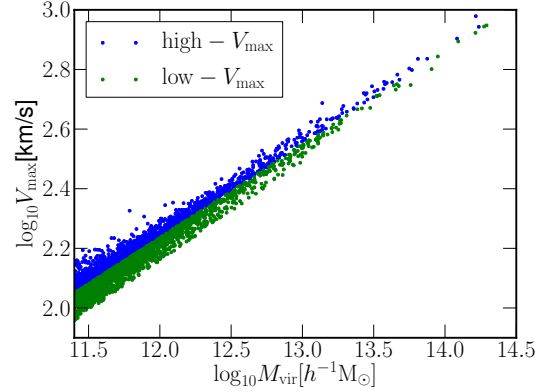


**Figure 1.** Distribution of halo mass and maximum circular velocity at  $z = 0$  for halos from the Bolshoi simulation. The blue dots represent halos whose observed maximum circular velocity,  $V_{\max, \text{obs}}$ , is greater than  $\bar{V}_{\max}$ , while the green dots are the ones with smaller  $V_{\max, \text{obs}}$  than  $\bar{V}_{\max}$ . The boundary between blue and green dots correspond to  $\bar{V}_{\max}$  computed from Eq. 1.

$\sim 6.3\%$  at  $10^{13} h^{-1} M_\odot$ . The lower mass resolution of the MultiDark simulation prevents us from making this additional subclassification. Accordingly, results that rely on this split are restricted to the Bolshoi simulation and mass range.

## 3 THE MAXIMUM CIRCULAR VELOCITY DEPENDENCE OF HALO CLUSTERING

In this section we present our primary results. We begin in §3.1 by describing the sample of halos we use throughout the paper, as well as our method for how we categorize halos as having above- or below-average circular velocities for their mass. In §3.2, we show the dependence of the clustering of halos on  $V_{\max}$ .

### 3.1 Halo Sample Definitions

If the internal structure of a dark matter halo of mass  $M_{\text{vir}}$  is described by an NFW profile (Navarro et al. 1997) of concentration  $c$ , then its maximum circular velocity  $V_{\max}$  is given by:

$$\bar{V}_{\max} = 0.465 M_{\text{vir}}^{1/3} \sqrt{G \left( \frac{4}{3} \pi \Delta_h \rho_{\text{crit}} \Omega_m \right)^{1/3} \frac{c}{\ln(1+c) - c/(1+c)}}. \quad (1)$$

As shown in (Klypin et al. 2011b), the median concentration-mass relation  $\bar{c}(M_{\text{vir}})$  for  $z = 0$  Bolshoi halos is well-described by:

$$\log_{10} \bar{c} = -0.097 \log_{10} M_{\text{vir}} + 2.148. \quad (2)$$

For every halo in the Bolshoi and MultiDark catalogs, we use its tabulated  $M_{\text{vir}}$  to compute  $\bar{c}(M_{\text{vir}})$ , and then use the values  $\bar{c}$  together with Eq. 1 to compute  $\bar{V}_{\max}$  for every halo. We will henceforth refer to halos with  $V_{\max} < \bar{V}_{\max}(M_{\text{vir}})$  as “low- $V_{\max}$  halos”, and halos with  $V_{\max} > \bar{V}_{\max}(M_{\text{vir}})$  as “high- $V_{\max}$  halos”. Thus a halo’s high- or low- $V_{\max}$  designation refers to whether its true  $V_{\max}$  value in the simulation is above- or below-average for its mass.

<sup>1</sup> <http://www.MultiDark.org>

<sup>2</sup> The catalogues used in this paper are publicly available at <http://hipacc.ucsc.edu/Bolshoi/MergerTrees.html>

Fig. 1 illustrates the distribution of Bolshoi halos as a function of  $M_{\text{vir}}$  and  $V_{\text{max}}$ . High- $V_{\text{max}}$  halos are shown in blue, low- $V_{\text{max}}$  halos in green. The dividing line between the two samples is defined by Eq. 1. We find that our analytical approximation for  $\bar{V}_{\text{max}}(M_{\text{vir}})$  gives a good description of the true median: for any fixed value of  $M_{\text{vir}}$ , the high- $V_{\text{max}}$  and low- $V_{\text{max}}$  subsamples have very similar numbers of objects.

Note that Fig. 1 shows a sharp lower bound on the value of  $V_{\text{max}}$  at a given  $M_{\text{vir}}$ , but no sharp upper bound. This is ultimately due to the halo mass definition. The circular velocity  $V_{\text{cir}}$  at the virial radius of any halo is  $V_{\text{cir}}(R_{\text{vir}}) \equiv V_{\text{vir}} = \sqrt{GM_{\text{vir}}/R_{\text{vir}}}$ . Since the value of  $V_{\text{max}}$  tabulated in the halo catalog is computed as the maximum value of  $V_{\text{cir}}$  over the entire profile of the halo, formally  $V_{\text{max}}$  cannot exceed  $V_{\text{vir}}$ . This manifests as the sharp lower bound seen in Fig. 1.

### 3.2 Halo Bias

In this section we present our primary results for the clustering properties of halos as a function of  $M_{\text{vir}}$  and  $V_{\text{max}}$ . Clustering strength is quantified by the two-point correlation function,  $\xi(r)$ . In all that follows, we will use  $\xi_{\text{mm}}(r)$  to denote the auto-correlation of the dark matter density field with itself, and  $\xi_{\text{hm}}(r)$  to denote the cross-correlation between a sample of halos and the underlying density field.

Halos are biased tracers of the dark matter density field. We denote this bias as  $b_{\text{h}}$ , which is in general a function of spatial separation. We define halo bias as

$$b_{\text{h}}(r) \equiv \xi_{\text{hm}}(r)/\xi_{\text{mm}}(r).$$

On sufficiently large scales halo bias is approximately linear, and  $b_{\text{h}}(r)$  approaches a constant value  $b_{\text{h}}^{\text{lin}}$ .

In order to measure the bias of a sample of simulated halos for both Bolshoi and MultiDark simulations, we estimate  $\xi_{\text{mm}}(r)$  and  $\xi_{\text{hm}}(r)$  using a random down-sampling of  $10^6$  dark matter particles. For a given sample of halos, we estimate the value of  $b_{\text{h}}^{\text{lin}}$  exhibited by the sample as follows:

$$b_{\text{h}}^{\text{lin}} = \frac{1}{N_{\text{bin}}} \sum_i (\xi_{\text{hm}}(r_i)/\xi_{\text{mm}}(r_i)). \quad (3)$$

In Eq. 3, the sum is performed over  $N_{\text{bin}} = 20$  separation bins  $r_i$  linearly spaced from  $10h^{-1}$  Mpc to  $20h^{-1}$  Mpc.

In order to study the mass-dependence of halo bias, we bin our halos into a sequence of  $M_{\text{vir}}$  bins chosen such that there are the same numbers of halos in each bin. For MultiDark, we select  $2 \times 10^5$  halos for each bin; for Bolshoi we use 25000 halos per bin. The halos in each mass bin are categorized as high- $V_{\text{max}}$  or low- $V_{\text{max}}$  according to the method described in §3.1. We start using halos from the MultiDark simulation for  $M_{\text{vir}} > 10^{12.2} h^{-1} M_{\odot}$ .

The top panel of Fig. 2 shows  $b_{\text{h}}^{\text{lin}}$  as a function of  $M_{\text{vir}}$ ; results for high- $V_{\text{max}}$  halos are shown in blue, low- $V_{\text{max}}$  halos in green. At the low-mass end, linear bias is a weak function of  $M_{\text{vir}}$ ; for  $M_{\text{vir}} \gtrsim M_{\text{coll}} \approx 10^{12.8} M_{\odot}/h$ , where  $M_{\text{coll}}$  is a characteristic mass scale for clustering corresponding to  $\sigma(M_{\text{coll}}, z) = \delta_c \approx 1.69$ , we see that  $b_{\text{h}}^{\text{lin}}$  increases sharply with  $M_{\text{vir}}$ . Thus the basic shape of each curve in Fig. 2 is in accord with theoretical expectations from the peak-background split (Sheth & Tormen 1999) formalism and Press-Schechter theory (Press & Schechter 1974). By comparing the blue and green curves in Fig. 2 we can see that linear bias has significant

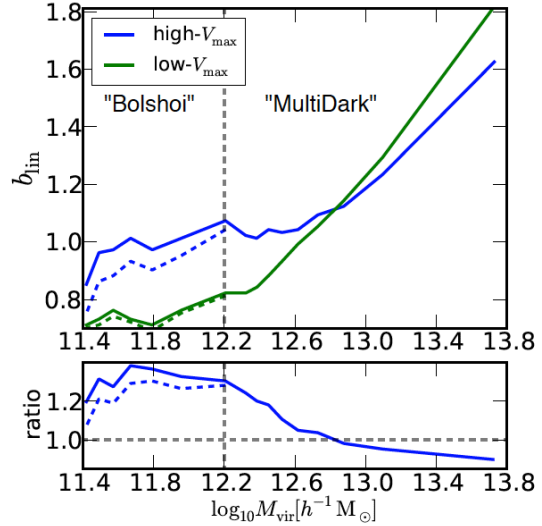


**Figure 2.** Upper panel: Linear bias at  $z = 0$  as a function of halo mass from the Bolshoi and the MultiDark simulations. The vertical dashed line indicates the upper/lower limit of halo mass for the Bolshoi/MultiDark simulations respectively. The blue lines correspond to a linear bias for high- $V_{\text{max}}$  halos, while the green lines correspond to low- $V_{\text{max}}$  halos. The solid lines correspond to the full halo sample while the dashed line corresponds to the sample where ejected halos are removed. Lower panel: Ratio of linear biases between high- $V_{\text{max}}$  and low- $V_{\text{max}}$  samples from the Bolshoi and the MultiDark simulations. The clustering difference increases with decreasing  $M_{\text{vir}}$ , and exceeds 30% for halos of Milky Way mass  $M_{\text{vir}} \approx 10^{12} M_{\odot}/h$ .

dependence upon  $V_{\text{max}}$  for halos of the same mass. This dependence is most readily seen in the bottom panel, which shows the ratio of  $b_{\text{h}}^{\text{lin}}$  of high- $V_{\text{max}}$  samples divided by  $b_{\text{h}}^{\text{lin}}$  of low- $V_{\text{max}}$  samples. Thus in the bottom panel of Fig. 2, vertical axis values exceeding unity correspond to masses where high- $V_{\text{max}}$  halos cluster more strongly relative to their low- $V_{\text{max}}$  counterparts.

At the low-mass end, high- $V_{\text{max}}$  halos are more strongly clustered than low- $V_{\text{max}}$  halos of the same mass. The clustering difference increases with decreasing  $M_{\text{vir}}$ , and exceeds 30% for halos of Milky Way mass  $M_{\text{vir}} \approx 10^{12} M_{\odot}/h$ . At the high-mass end, the trend reverses, and the overall magnitude is weaker. These results are consistent with Wechsler et al. (2006), who find that the same trends hold when the secondary halo property is NFW concentration, rather than  $V_{\text{max}}$ . This agreement is to be expected: insofar as the halo profile is well-approximated by an NFW profile,  $V_{\text{max}}$  is entirely determined by concentration (see Eq. 1). Note that there is a drop in the ratio of the linear biases on the low-mass end. As we see no physical reason for this drop, we consider this to be a resolution effect and suggest that the completeness requirements for two-halo-property-dependent clustering are significantly more stringent relative to the requirements demanded by the need for a complete halo mass/velocity function.

Next, we study the scale-dependence of halo bias on small scales for high- $V_{\text{max}}$  and low- $V_{\text{max}}$  halos. We wish to parse the novel, small-scale effects from the well-known large-scale effects. So for each sample of high- and low- $V_{\text{max}}$  halos, we compute the following quantity:

$$\tilde{b}_h(r|M_{\text{vir}}; V_{\text{max}}) \equiv b_h(r|M_{\text{vir}}; V_{\text{max}})/b_{\text{lin}}(M_{\text{vir}}; V_{\text{max}}). \quad (4)$$

Thus for any sample of halos, as  $r \gtrsim 10\text{Mpc}/h$ , we have  $\tilde{b}_h(r) \rightarrow 1$ , by construction.

The bottom panel of Fig. 3 shows the ratio of  $\tilde{b}_h(r)$  of high- $V_{\text{max}}$  samples divided by  $b_h(r)$  of low- $V_{\text{max}}$  samples for several mass bins. The first three mass bins labeled in the figure,  $M_{\text{vir}} = 10^{11.7, 12.0, 12.2} h^{-1} M_{\odot}$ , are from the Bolshoi simulation, and the last two mass bins,  $M_{\text{vir}} = 10^{12.7, 13.1} h^{-1} M_{\odot}$ , are from the MultiDark simulation. High- $V_{\text{max}}$  halos cluster more strongly compared to their low- $V_{\text{max}}$  counterparts at  $1h^{-1}\text{Mpc}$ . This scale-dependent feature becomes stronger with decreasing  $M_{\text{vir}}$  and exceeds 40% for halos of Milky Way mass and reaches 60% at  $M_{\text{vir}} \approx 10^{11.7} h^{-1} M_{\odot}$ .

Up until present, we have used both host halos and ejected halos to compute halo biases. Both types of halos are identified as distinct halos at  $z = 0$ . Ejected halos, however, are halos which were identified as part of more massive halos at one or more occasions in the past, but were ejected and now exist as a host halo at  $z = 0$ . Those ejected halos tend to exist around more massive halos (Wetzel et al. 2014; Wang et al. 2009, e.g.). Therefore, the effect on scale-dependent biases may be caused by those ejected halos.

To test this ejected halo hypothesis, we compute halo-matter cross correlation functions after first excluding the sub-population of ejected halos. Our results for the linear regime are shown as the dashed curves in Fig. 2. The relative difference in the linear bias between high- $V_{\text{max}}$  and low- $V_{\text{max}}$  halos is suppressed to 25% for halos of Milky Way mass. This suppression due to excluding the ejected halos is consistent with the results presented in Wang et al. (2009).

In the bottom panel of Fig. 3, we show the scale-dependence of assembly bias for non-ejected halos.<sup>3</sup> Once the ejected halos have been removed, the scale-dependent feature of assembly bias is greatly reduced. This implies an intimate connection between the scale-dependence of assembly bias and subhalo back-splashing (see §5 for further discussion).

#### 4 OBSERVATIONAL CONSEQUENCES

We now consider possible observational consequences of the results of the previous section. In order to do this, the key first step is to relate an observable property of a galaxy (luminosity, stellar mass) to an intrinsic property of its host halo (mass, circular velocity). As one might infer from above (and we demonstrate below), different choices for the latter can result in significant differences for different observables.

In order to be explicit, we use the abundance matching technique (Kravtsov et al. 2004; Vale & Ostriker 2004; Tasitomi et al. 2004; Vale & Ostriker 2006; Conroy & Wechsler 2009; Guo et al. 2010; Simha et al. 2010; Neistein et al. 2010; Watson et al. 2012; Rodríguez-Puebla et al. 2012; Kravtsov 2013) to connect the stellar masses of central galaxies to either the mass or circular velocity of host halos. We implement this by splitting the halo catalog into a series of bins with constant

<sup>3</sup> We remind the reader that due to the mass resolution of the MultiDark simulation, fig. 3 only shows results for Bolshoi halos.

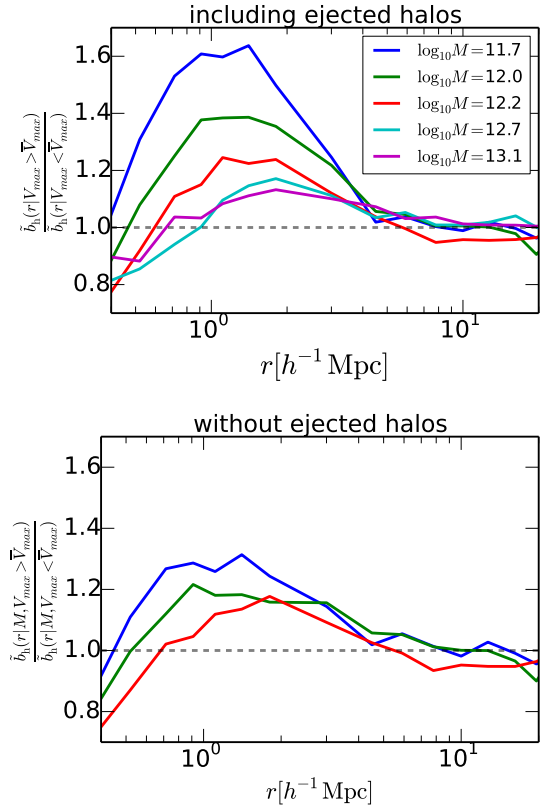


**Figure 3.** Top panel: Ratio of halo-matter cross correlation functions between high/low- $V_{\text{max}}$  halos from the Bolshoi simulation and the MultiDark simulation at  $z = 0$ , normalized by their linear biases. Each line corresponds to different halo mass bins labeled in the plots. The top three lines that correspond to low mass halos are computed from halos in the Bolshoi simulation, while the bottom lines are from the MultiDark simulation. Those plots show that high- $V_{\text{max}}$  halos cluster more strongly than low- $V_{\text{max}}$  halos at  $1h^{-1}\text{Mpc}$  and the relative scale-dependence between those subsamples increases smoothly with decreasing halo mass. Bottom panel: The same figure as the top panel without ejected halos only from the Bolshoi simulation. As can be seen by comparing these results to those in the top panel, the  $V_{\text{max}}$ -dependence of halo bias on small scales is dramatically reduced by excluding ejected subhalos. This implies an intimate connection between the scale-dependence of assembly bias and subhalo back-splashing.

number density ( $=1.6 \times 10^{-3} (h^{-1}\text{Mpc})^{-3}$ ), rank ordering either by mass or circular velocity. We label each bin by its corresponding stellar mass, computed from the stellar-to-halo mass relation of (Behroozi et al. 2013a).

Note that when we rank order based on circular velocity, there is the possibility that the mean halo masses of these bins could differ from what we obtain after rank ordering by halo mass. We explicitly check this and find that the mean halo masses for both cases agree to  $\sim 99.6\%$ , allowing us to consistently compare samples of mock central galaxies with the same stellar mass, but where the stellar mass is statistically regulated by either  $M_{\text{vir}}$  or  $V_{\text{max}}$ .

We find only a relatively minor difference in the large-scale clustering of the two samples of mock central galaxies. At fixed stellar mass, the linear bias of samples selected by their circular velocity are  $\sim 5\%$  higher than samples selected by halo mass.

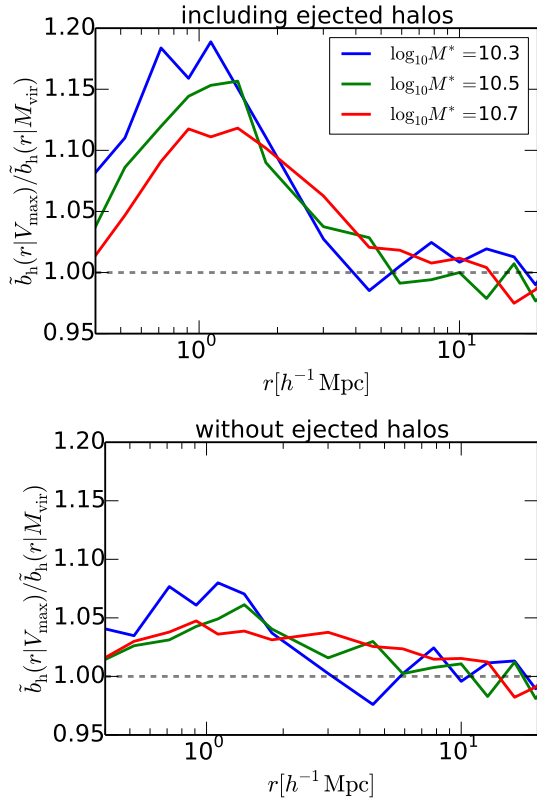


**Figure 4.** Ratio of halo-matter cross correlation functions between  $M_{\text{vir}}$ -based and  $V_{\text{max}}$ -based abundance matching samples with ejected halos (top) and without ejected halos (bottom). The ratios are normalized by their linear biases. Each line corresponds to different stellar mass bins labeled in the plots. With ejected halos, the halo biases computed from the  $V_{\text{max}}$ -selected samples have very different scale-dependence than the ones from the  $M_{\text{vir}}$ -selected samples. By removing those ejected halos, the difference is reduced by threefold.

This decreases to  $\sim 2\%$  if we remove ejected halos from both samples.

We study the scale-dependence of the clustering of our mock central galaxies in Fig. 4, which is directly analogous to Fig. 3, only here we have use the abundance matching technique described above to illustrate how our “halo-level” results may manifest in observed galaxy populations. Again we see a clear scale-dependence of the clustering signal, with a maximum difference of  $\sim 15\%$  at  $\sim 1h^{-1}\text{Mpc}$ . These differences go down to  $\sim 5\%$  after removing ejected subhalos, again reflecting the intimate connection between scale-dependent assembly bias and subhalo back-splashing.

## 5 DISCUSSION

For halos  $M_{\text{vir}} \gtrsim M_{\text{coll}} \approx 10^{12.8} M_{\odot}/h$ , we have shown that the linear bias of low- $V_{\text{max}}$  halos is larger relative to high- $V_{\text{max}}$  halos of the same mass. As shown in Dalal et al. (2008), this phenomenon is nicely explained in terms of the statistics of fluctuations in a Gaussian random field. Consider two halos with the same present-day mass, but with different concentration. Both halos originate from a fluctuation of the same peak height, but with different peak curvature: the high-concentration

(high- $V_{\text{max}}$ ) halo has a sharper peak than the low-concentration (low- $V_{\text{max}}$ ) halo. Dalal et al. (2008) showed that a generic prediction of Extended Press Schechter theory (EPS) with a configuration space filter is that low-curvature peaks cluster more strongly relative to high-curvature peaks of the same height. In closely related work, Zentner (2007) used EPS with a configuration space filter to show that for a pair of halos of the same peak height, the early-forming halo should reside in a denser large-scale environment than the late-forming one.<sup>4</sup>

A critical assumption underlying these EPS predictions is that a halo is the dominant peak in its large-scale environment. This is a well-founded assumption at the high-mass end, and we see that the predictions are in good agreement with simulations in the  $M_{\text{vir}} > M_{\text{coll}}$  regime (Dalal et al. 2008). The situation is quite different when  $M_{\text{vir}} \lesssim M_{\text{coll}}$ . We have confirmed previous results (e.g., Wechsler et al. 2006) that large-scale assembly bias changes sign and strengthens for lower-mass halos. This is in stark contrast to the EPS model described above, which makes the same prediction for assembly bias regardless of halo mass.

Thus EPS succeeds and fails in precisely the regimes where we expect. Lower-mass halos are strongly influenced by the tidal field in which they evolve (Hahn et al. 2007; Wang et al. 2011; Shi et al. 2015; Hahn et al. 2009; Hearin et al. 2015); the EPS assumption that the halo dominates its environment breaks down catastrophically, and in this regime nonlinear evolution governs assembly bias. On the other hand, high-mass halos *do* dominate their tidal environment; the EPS assumption holds good, and we can understand assembly bias as naturally arising from the statistics of Gaussian fluctuations.

Our results on the scale-dependence of assembly bias are also consistent with this picture. First, we remind the reader that halo bias for high- $V_{\text{max}}$  halos shows non-trivial scale dependence with a pronounced bump at  $\sim 1 - 2\text{Mpc}/h$  compared to the bias for low- $V_{\text{max}}$  halos. This scale-dependent feature for high- $V_{\text{max}}$  halos becomes 60% larger compared to low- $V_{\text{max}}$  halos at  $M_{\text{vir}} \approx 10^{11.7} M_{\odot}/h$ . This feature, however, is removed by excluding the ejected halos, implying that this special sub-population is responsible for the scale-dependent bump.

This scale-dependence has a simple interpretation in terms of subhalo back-splashing. First, ejected halos are physically associated with the more massive halo from which they were ejected. The clustering of ejected halos is therefore largely determined by this associated massive halo, much like the clustering of present-day subhalos is determined by their host halo. Second, as ejected halos pass near and inside a massive halo, their physical growth is arrested, and many such halos even experience substantial mass loss (Wang et al. 2009; Wetzel et al. 2014). This arrested development has a greater impact on the outer layers of the halo, so that the ejected halo’s mass is significantly more affected than its circular velocity (Behroozi et al. 2013b). Putting these two effects together, we should naturally expect the outskirts of massive groups and clusters to be preferentially populated with low-mass halos that have above-average values of  $V_{\text{max}}$  for their mass. This manifests in the scale-dependent bump shown in Figures 3 & 4.

Recent advances in our understanding of halo growth sheds further light on the above results. As shown in Diemer & Kravtsov (2014); Adhikari et al. (2014); Wetzel & Nagai

<sup>4</sup> See Chapter IX, Section D.

(2014); More et al. (2015), the natural physical boundary of a dark matter is the so-called “splashback radius”, which is the radius where accreted matter reaches its first apocenter after turnaround, and is roughly  $2 - 3R_{\text{vir}}$ . As shown in Wetzel et al. (2014), the halos of massive groups and clusters ( $M_{\text{vir}} \gtrsim 10^{13} M_{\odot}/h$ ,  $R_{\text{vir}} \gtrsim 500 \text{kpc}/h$ ) are surrounded by a large fraction of ejected halos. For ejected halos with  $M_{\text{vir}} \approx 10^{11.7} h^{-1} M_{\odot}$  halos, the host-centric spatial distribution of the ejected population peaks at  $r \approx 1.25 R_{200\text{m}} \approx 1.5 \text{Mpc}/h$  (see Figs. 2 and 3 in Wetzel et al. (2014)). The bump feature we find at  $1 - 2 \text{Mpc}/h$  is therefore in quantitative agreement with the Wetzel et al. (2014); Wang et al. (2007) results: this bump occurs at the same physical scale that we would expect if the clustering of the ejected population is largely determined by the host to which the halos are ultimately bound. Note that the assembly bias on large scales,  $r \gtrsim 10 \text{Mpc}/h$ , is not dominated by the ejected halos, which is consistent with Wang et al. (2007). Without the ejected halos, the relative difference in the linear bias between high- $V_{\text{max}}$  and low- $V_{\text{max}}$  halos remains 25% for halos of Milky Way mass.

In order to explore possible observational consequences of our findings, we use abundance matching relating a stellar mass of central galaxies to either mass or circular velocity of host halos. Using different intrinsic properties for host halos results in significant differences in clustering signals of central galaxies. On large scales, the linear bias of samples selected by their circular velocities are  $\sim 5\%$  higher than samples selected by halo masses at fixed stellar mass. Without the ejected halos, this difference is reduced to  $\sim 2\%$ . On small scales ( $r < 10 h^{-1} \text{Mpc}$ ), samples selected by their circular velocities exhibit the scale dependence with a bump at  $1 - 2 h^{-1} \text{Mpc}$  compared to samples selected by halo masses. This scale-dependent bump for  $V_{\text{max}}$ -selected samples becomes  $\sim 15\%$  with the ejected halos and  $\sim 5\%$  without the ejected halos. As these effects are roughly as large as existing SDSS clustering measurements on these scales, this raises the possibility that clustering measurements can be used to determine which host halo property is the true statistical regulator of the stellar mass of the central galaxy residing in the halo.

## 6 SUMMARY

We conclude the paper with an overview of our primary results:

(i) At fixed mass  $M_{\text{vir}}$ , the large-scale bias of halos exhibits significant residual dependence on potential well depth  $V_{\text{max}}$ . At the low-mass end, high- $V_{\text{max}}$  halos cluster more strongly than their low- $V_{\text{max}}$  counterparts. At the high-mass end, this trend reverses, and is generally weaker, with the transition occurring at  $M_{\text{coll}} \approx 10^{12.5} M_{\odot}/h$ . Our results are quantitatively consistent with previous studies of large-scale halo assembly bias.

(ii) We show that assembly bias exhibits complex scale-dependence. The  $V_{\text{max}}$ -dependence of halo clustering shows a pronounced “bump” on scales  $500 \text{kpc}/h \lesssim r \lesssim 5 \text{Mpc}/h$ . This scale-dependence is itself mass-dependent: the bump feature is strongest for low-mass halos and vanishes for halos with  $M_{\text{vir}} \gtrsim M_{\text{coll}}$ .

(iii) The scale-dependence of assembly bias can primarily be attributed to a special sub-population of *ejected subhalos*, which experience arrested mass-growth before and after being ejected

from a higher-mass host. If this special population is excluded from the halo sample, the strength of small-scale assembly bias is limited to  $\lesssim 5\%$  for all masses  $M_{\text{vir}} \gtrsim 10^{11.75} M_{\odot}/h$ .

## 7 ACKNOWLEDGEMENTS

We thank Andrew Zentner and Frank van den Bosch for informative conversations. A portion of this work was supported by the National Science Foundation under grant PHYS-1066293 and the hospitality of the Aspen Center for Physics.

## REFERENCES

- Adhikari S., Dalal N., Chamberlain R. T., 2014, JCAP, 11, 19  
 Behroozi P. S., Wechsler R. H., Conroy C., 2013a, ApJ, 770, 57  
 Behroozi P. S., Wechsler R. H., Lu Y., Hahn O., Busha M. T., Klypin A., Primack J. R., 2013b, ArXiv:1310.2239  
 Behroozi P. S., et al., 2013c, ApJ, 763, 18  
 Behroozi P. S., et al., 2013d, ApJ, 762, 109  
 Berlind A. A., Weinberg D. H., 2002, ApJ, 575, 587  
 Berlind A. A., et al., 2003, ApJ, 593, 1  
 Bullock J. S., Kolatt T. S., Sigad Y., Somerville R. S., Kravtsov A. V., Klypin A. A., Primack J. R., Dekel A., 2001, MNRAS, 321, 559  
 Cacciato M., van den Bosch F. C., More S., Mo H., Yang X., 2013, MNRAS, 430, 767  
 Conroy C., Wechsler R. H., 2009, ApJ, 696, 620  
 Dalal N., White M., Bond J. R., Shirokov A., 2008, ApJ, 687, 12  
 Diemer B., Kravtsov A. V., 2014, ApJ, 789, 1  
 Faltenbacher A., White S. D. M., 2010, ApJ, 708, 469  
 Gao L., Springel V., White S. D. M., 2005, MNRAS, 363, L66  
 Gao L., White S. D. M., 2007, MNRAS, 377, L5  
 Geach J. E., Sobral D., Hickox R. C., Wake D. A., Smail I., Best P. N., Baugh C. M., Stott J. P., 2012, MNRAS, 426, 679  
 Gottloeber S., Klypin A., 2008, ArXiv:0803.4343  
 Guo Q., White S., Li C., Boylan-Kolchin M., 2010, MNRAS, 404, 1111  
 Hahn O., Carollo C. M., Porciani C., Dekel A., 2007, MNRAS, 381, 41  
 Hahn O., Porciani C., Dekel A., Carollo C. M., 2009, MNRAS, 398, 1742  
 Hearin A. P., Behroozi P. S., van den Bosch F. C., 2015, ArXiv:1504.05578  
 Hearin A. P., Zentner A. R., Berlind A. A., Newman J. A., 2012, ArXiv:1210.4927  
 Klypin A. A., Trujillo-Gomez S., Primack J., 2011a, ApJ, 740, 102  
 Klypin A. A., Trujillo-Gomez S., Primack J., 2011b, ApJ, 740, 102  
 Kravtsov A. V., 2013, ApJ, 764, L31  
 Kravtsov A. V., Berlind A. A., Wechsler R. H., Klypin A. A., Gottlöber S., Allgood B., Primack J. R., 2004, ApJ, 609, 35  
 Kravtsov A. V., Klypin A. A., Khokhlov A. M., 1997, ApJS, 111, 73  
 Leauthaud A., Tinker J., Behroozi P. S., Busha M. T., Wechsler R. H., 2011, ApJ, 738, 45  
 Leauthaud A. et al., 2012, ApJ, 744, 159  
 Li Y., Mo H. J., Gao L., 2008, MNRAS, 389, 1419

- Magliocchetti M., Porciani C., 2003, *MNRAS*, 346, 186
- Mandelbaum R., Slosar A., Baldauf T., Seljak U., Hirata C. M., Nakajima R., Reyes R., Smith R. E., 2013, *MNRAS*, 432, 1544
- Mo H., van den Bosch F. C., White S., 2010, *Galaxy Formation and Evolution*. Cambridge University Press
- More S., Diemer B., Kravtsov A., 2015, *ArXiv e-prints*
- More S., van den Bosch F. C., Cacciato M., More A., Mo H., Yang X., 2013, *MNRAS*, 430, 747
- Navarro J. F., Frenk C. S., White S. D. M., 1997, *ApJ*, 490, 493
- Neistein E., Weinmann S. M., Li C., Boylan-Kolchin M., 2010, *ArXiv:1011.2492*
- Parejko J. K. et al., 2013, *MNRAS*, 429, 98
- Prada F., Klypin A. A., Cuesta A. J., Betancort-Rijo J. E., Primack J., 2011, *ArXiv e-prints*
- Press W. H., Schechter P., 1974, *ApJ*, 187, 425
- Riebe K. et al., 2011, *ArXiv:1109.0003*
- Rodríguez-Puebla A., Drory N., Avila-Reese V., 2012, *ApJ*, 756, 2
- Ross A. J., Percival W. J., Brunner R. J., 2010, *MNRAS*, 407, 420
- Saito S. et al., 2015, *ArXiv:1509.00482*
- Seljak U., 2000, *MNRAS*, 318, 203
- Sheth R. K., Tormen G., 1999, *MNRAS*, 308, 119
- Shi J., Wang H., Mo H., 2015, *ArXiv:1501.07764*
- Simha V., Weinberg D., Dave R., Fardal M., Katz N., Oppenheimer B. D., 2010, *ArXiv:1011.4964*
- Simon P., Hettterscheidt M., Wolf C., Meisenheimer K., Hildebrandt H., Schneider P., Schirmer M., Erben T., 2009, *MNRAS*, 398, 807
- Skibba R. A., 2009, *MNRAS*, 392, 1467
- Tasitsiomi A., Kravtsov A. V., Wechsler R. H., Primack J. R., 2004, *ApJ*, 614, 533
- Tinker J. L., Weinberg D. H., Zheng Z., Zehavi I., 2005, *ApJ*, 631, 41
- Vale A., Ostriker J. P., 2004, *MNRAS*, 353, 189
- Vale A., Ostriker J. P., 2006, *MNRAS*, 371, 1173
- van den Bosch F. C. et al., 2007, *MNRAS*, 376, 841
- Wang H., Mo H. J., Jing Y. P., 2009, *MNRAS*, 396, 2249
- Wang H., Mo H. J., Jing Y. P., Yang X., Wang Y., 2011, *MNRAS*, 413, 1973
- Wang H. Y., Mo H. J., Jing Y. P., 2007, *MNRAS*, 375, 633
- Watson D. F., Berlind A. A., Zentner A. R., 2012, *ApJ*, 754, 90
- Wechsler R. H., Bullock J. S., Primack J. R., Kravtsov A. V., Dekel A., 2002, *ApJ*, 568, 52
- Wechsler R. H., Zentner A. R., Bullock J. S., Kravtsov A. V., Allgood B., 2006, *ApJ*, 652, 71
- Wetzel A. R., Nagai D., 2014, *ArXiv:1412.0662*
- Wetzel A. R., Tinker J. L., Conroy C., Bosch F. C. v. d., 2014, *MNRAS*, 439, 2687
- Yang X., Mo H. J., van den Bosch F. C., 2003, *MNRAS*, 339, 1057
- Yang X., Mo H. J., van den Bosch F. C., Weinmann S. M., Li C., Jing Y. P., 2005, *MNRAS*, 362, 711
- Zehavi I., et al., 2005, *ApJ*, 630, 1
- Zehavi I., et al., 2011, *ApJ*, 736, 59
- Zentner A. R., 2007, *International Journal of Modern Physics D*, 16, 763
- Zentner A. R., Hearin A. P., van den Bosch F. C., 2013, *ArXiv:1311.1818*
- Zheng Z., Coil A. L., Zehavi I., 2007, *ApJ*, 667, 760
- Zheng Z., Zehavi I., Eisenstein D. J., Weinberg D. H., Jing Y. P., 2009, *ApJ*, 707, 554